



Magnetism of intermediate hydromaghemite in the transformation of 2-line ferrihydrite into hematite and its paleoenvironmental implications

Qingsong Liu,¹ Vidal Barrón,² José Torrent,² Sigrid G. Eeckhout,³ and Chenglong Deng⁴

Received 4 June 2007; revised 14 October 2007; accepted 2 November 2007; published 22 January 2008.

[1] A maghemite-like phase referred to here as “hydromaghemite” was obtained as an intermediate product in the hydrothermal transformation of phosphated 2-line ferrihydrite into hematite. In this study, we used magnetic and non-magnetic (e.g., X-ray Absorption Near Edge Structure, XANES) techniques in combination to characterize a series of the intermediate products obtained in the aging of phosphated ferrihydrite (P/Fe atomic ratio = 0.03) at 150°C for 120 days. Particle size calculated from both the specific surface area and average unblocking temperature increased with time. XANES spectra revealed the presence of some tetrahedrally coordinated iron, which is consistent with the formation of hydromaghemite (the dominant magnetic phase in the intermediate products). Thus grain size in newly formed hydromaghemite particles increased with time from the initial values in the superparamagnetic region to others in the single-domain region. Further transformation of hydromaghemite into hematite, which was complete by day 120, was probably due to hydromaghemite becoming unstable relative to hematite when the surface to volume ratio fell below a given threshold. The relationships between pedogenically produced maghemite and hematite contents in various soils and paleosols suggest that the ferrihydrite → hydromaghemite → hematite transformation may constitute a major pathway accounting for the magnetic enhancement in many soils.

Citation: Liu, Q., V. Barrón, J. Torrent, S. G. Eeckhout, and C. Deng (2008), Magnetism of intermediate hydromaghemite in the transformation of 2-line ferrihydrite into hematite and its paleoenvironmental implications, *J. Geophys. Res.*, *113*, B01103, doi:10.1029/2007JB005207.

1. Introduction

[2] Magnetite and maghemite are the two dominant ferrimagnetic minerals responsible for soil magnetism [Mullins, 1977; Maher, 1986; Schwertmann and Taylor, 1989; Verosub et al., 1993; Singer et al., 1996; Maher, 1998; Barrón and Torrent, 2002; Liu et al., 2004a, 2005a, 2007]. The origin of maghemite in soils is complex relative to magnetite. Maghemite can form by (1) oxidation of fine-grained magnetite [Murad and Schwertmann, 1993]; (2) partial oxidation of coarse-grained magnetite producing a maghemite rim [van Velzen and Dekkers, 1999a, 1999b; Liu et al., 2004a]; (3) heating of goethite (α -FeOOH) in the presence of organic matter [Schwertmann and Taylor, 1989]; and (4) thermal conversion of lepidocrocite [Banin et al., 1993; Morris et al., 1998]. However, the temperatures required for thermal conversion of precursor Fe hydr(ox-

ides) are only reached in special situations (e.g., in soil in contact with a burning tree stump).

[3] Maghemite can also be readily prepared in the laboratory by heating ferrihydrite above 250°C in flowing N₂ [Eggleton and Fitzpatrick, 1988]. Barrón and Torrent [2002] found hydrothermal aging of phosphated 2-line ferrihydrite at 150–200°C under oxidizing conditions to produce a maghemite-like phase (hereafter referred to as “hydromaghemite”) that was later transformed into hematite [Barrón and Torrent, 2002]. Detailed X-ray diffraction (XRD), transmission electron microscopy (TEM), visible diffuse reflectance and Mössbauer spectroscopy, and low-field magnetic susceptibility measurements by Barrón and Torrent [2002] and Barrón et al. [2003], showed the initial phosphated 2-line ferrihydrite to be gradually transformed into the hydromaghemite phase, which consisted of sub-rounded particles 10–30 nm in size that appeared homogeneous under the TEM. The XRD patterns and Mössbauer spectra were consistent with this product being a mixture of 2- and 6-line ferrihydrite and maghemite. In experiments at 150°C, the magnetic susceptibility of bulk samples first gradually increased to a maximum at 90 days and then abruptly decreased by ~2 orders of magnitude at 120 days by effect of the transformation of maghemite into hematite.

[4] The transformation of 2-line ferrihydrite into hydromaghemite is likely to be favored by the former having

¹National Oceanography Centre, University of Southampton, Southampton, UK.

²Departamento de Ciencias y Recursos Agrícolas y Forestales, Universidad de Córdoba, Córdoba, Spain.

³European Synchrotron Radiation Facility (ESRF), Grenoble, France.

⁴Paleomagnetism and Geochronology Laboratory (SKL-LE), Institute of Geology and Geophysics, Chinese Academy of Sciences, Beijing, China.

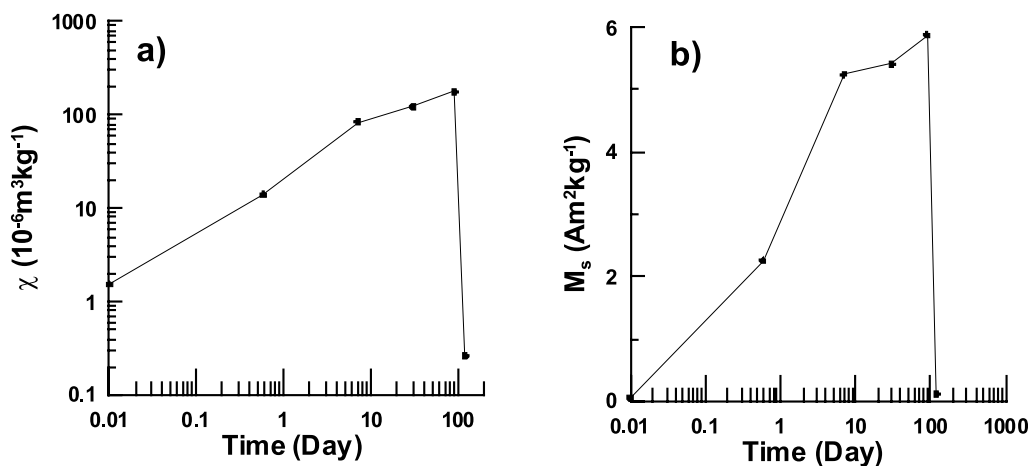


Figure 1. Magnetic susceptibility χ (a) and saturation magnetization M_s (b) as a function of aging time for the products formed from phosphated ferrihydrite in a ligand/Fe ratio of 0.03.

tetrahedral Fe in a maghemite-like structure [Janney *et al.*, 2000]. High-energy X-ray total scattering observations [Michel *et al.*, 2007a, 2007b] suggest that synthetic ferrihydrites with coherently scattering domains of approximately 2, 3, and 6 nm possess a hexagonal unit cell which, in its ideal form, consists of 20% tetrahedrally and 80% octahedrally coordinated Fe. The presence of tetrahedral Fe may thus favor the transformation of various ferrihydrites into maghemite-like phases. However, aging 6-line ferrihydrite produced hematite and/or goethite, but no ferrimagnetic phases [Mazzetti and Thistlethwaite, 2002; Barrón *et al.*, 2003]. The origin of the difference between 2- and 6-line ferrihydrites may reside, among other factors, in the fact that surface relaxation increases with decreasing particle size [Michel *et al.*, 2007a]. For small particles, progressive structural rearrangement into a more ordered phase is therefore possible (provided a sufficient amount of strongly adsorbing ligands block the ferrihydrite surface and hinder the thermodynamically favorable, fast formation of hematite and goethite [Barrón and Torrent, 2002]). In summary, poor crystallinity and the presence of strongly sorbing ligands seem to be two necessary conditions for the transformation of ferrihydrite into hydromaghemite.

[5] The objective of this study was to characterize in detail the magnetic properties and grain size of the magnetic phases in the intermediate products of the hydrothermal transformation of phosphated 2-line ferrihydrite. Low-temperature magnetic techniques allowed us to detect subtle changes in grain size in hydromaghemite particles during the transformation process. These results are used here to discuss how critical the influence of grain size on the transformation of hydromaghemite into hematite is. The paleoenvironmental implications of this transformation are also discussed.

2. Sample Descriptions and Experiments

2.1. Sample Descriptions

[6] The samples used in this study were among those previously prepared by Barrón and Torrent [2002]. The initial 2-line ferrihydrite was synthesized by precipitating 0.01 M $\text{Fe}(\text{NO}_3)_3$ with 1 M KOH to a final pH of 7. The

initial solution contained phosphate at a P/Fe atomic ratio of 0.03, which was previously found to result in maximal formation of hydromaghemite (only hematite was formed at $\text{P/Fe} < 0.02$ and no ferrihydrite was transformed at $\text{P/Fe} > 0.05$, Barrón and Torrent [2002]). Five ferrihydrite suspensions were aged in polytetrafluorethylene-lined vessels that were placed in an oven at 150°C and removed at 12 h and also at 7, 30, 90, and 120 days. After cooling, the suspension was centrifuged at $1.5 \times 10^4 \text{ m s}^{-2}$ for 10 min, the supernatant decanted, and the sediment washed several times with deionized water to remove salts prior to freeze-drying. For a more detailed description of the synthetic procedure, X-ray patterns and Mössbauer spectra for the products, interested readers are referred to Barrón and Torrent [2002] and Barrón *et al.* [2003].

[7] The specific surface area (SSA) of the products, calculated by using the BET method, was determined by N_2 adsorption on a Micromeritics ASAP 2010 equipment. For magnetic measurements, an amount of 5 mg of dry products was mixed with CaF_2 and packed into a gelatin capsule to minimize the potential effects of magnetic interactions.

2.2. Magnetic Experiments

[8] Room temperature hysteresis loops were obtained by using a Princeton Applied Research vibrating sample magnetometer (VSM 2900). The saturation field was 1 T. Saturation magnetization (M_s), saturation remanence (M_{rs}), and coercivity (B_c) were obtained after subtracting the paramagnetic contribution.

[9] Temperature-dependent low-field (10 mT) direct current (DC) susceptibility (hereafter denoted as low-T DC χ - T) between 5 and 300 K was measured with a Quantum Designs Magnetic Properties Measurement System (MPMS). First, about 5 mg sample was cooled to 5 K in a zero field; then, in the field of 10 mT, the sample was warmed up to 300 K and subsequently cooled down to 5 K. The temperature sweeping rate was 5 K min^{-1} and the corresponding errors due to thermal lags when sweeping less than $\pm 1 \text{ K}$. For the low-T DC χ - T curves, the average unblocking temperature $\langle T_B \rangle$ was defined as the temperature corresponding to the maximum susceptibility (see section 2.3 for details).

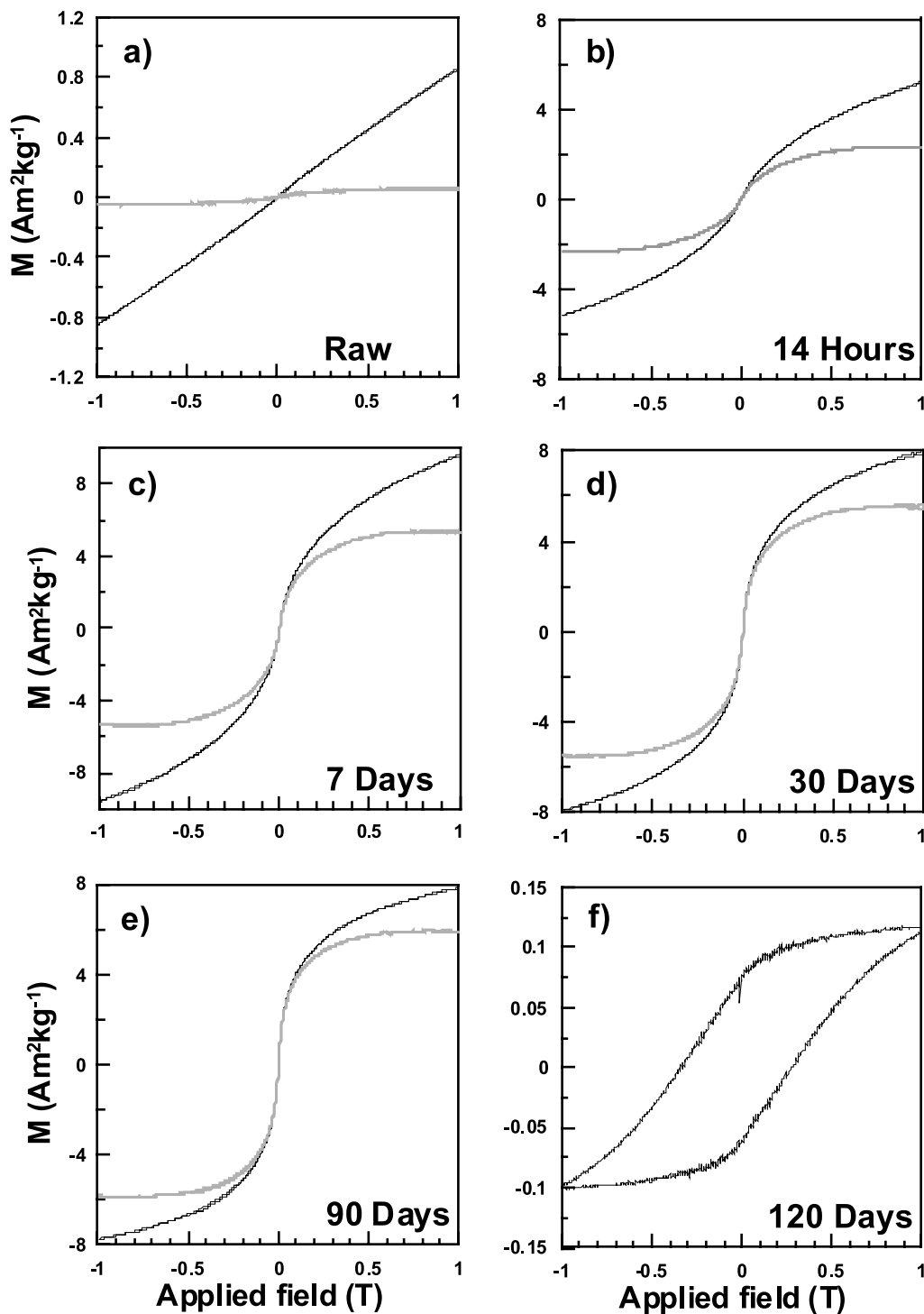


Figure 2. Hysteresis loops for the intermediate aging products. The dark and gray curves are the loops before and after correcting the linearly paramagnetic contributions.

[10] For the same sample, the stepwise temperature-dependence of low-field mass-specific magnetic susceptibility (χ) was determined by using a Kappa Bridge 3 instrument equipped with a CS-3 furnace at temperature from room level to values up to 700°C in an argon atmosphere (the flux rate was 100 ml/min). The maximum treatment temperature was named T_{tr} . The temperature step was 5°C. High-field thermomagnetic analyses ($M-T$, heating from room temperature to temper-

atures up to 700°C and cooling) were conducted with a Magnetic Measurements Variable Field Translation Balance (VFTB), using a steady field of 300 mT. Experiments were started with an amount of raw material of ~ 100 mg.

2.3. On the Use of $\langle T_B \rangle$ for Grain Size Analysis

[11] The mean unblocking temperature $\langle T_B \rangle$ of a fine ferrimagnetic or ferromagnetic particle system with a given

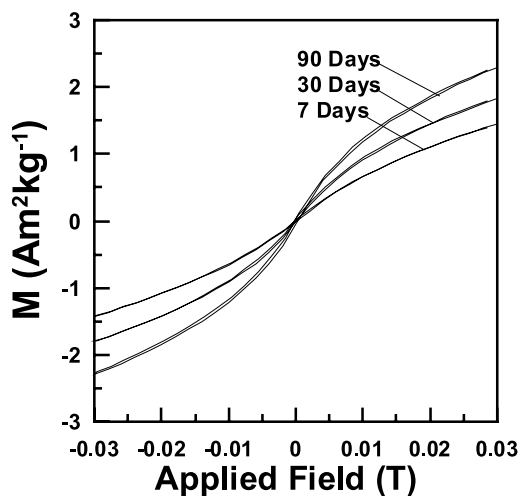


Figure 3. Comparison of the hysteresis loops for the 7-, 30- and 90-day intermediate products.

particle size distribution is generally proportional to the mean particle volume provided the anisotropy constant is invariable [Gittleman *et al.*, 1974; Khater *et al.*, 1987; El-Hilo *et al.*, 1992]. For a non-interacting system, the temperature dependence of the DC magnetic susceptibility increases with increasing temperature through an increasing fraction of particles that are gradually unblocked. On the other hand, thermal agitation reduces the susceptibility and gives rise to a peak at $\langle T_B \rangle$ [Gittleman *et al.*, 1974; Khater *et al.*, 1987].

[12] Based on the Néel theory, and on the assumption of temperature-independence in M_s and macroscopic coercivity (H_K) at <300 K, Jackson and Worm [2001] simulated the temperature-dependence of in-phase magnetic susceptibility. By using the same model (see Jackson and Worm [2001] for details), we constructed the relationship between grain size and $\langle T_B \rangle$ for maghemite. Liu *et al.* [2005b] showed the estimation of grain size to be less dependent on coercivity changes. For example, changes in coercivity by about 10% yield an error in the diameter of only about 3%. Moreover, the roughly spherical particle shape of the intermediate products suggests that the corresponding magnetic coercivity could only be slightly larger than 20 mT (the minimum coercivity controlled by the magnetocrystalline anisotropy for cubic single domain particles, Dunlop and Özdemir [1997]). Accordingly, we used a magnetic anisotropy constant of 40000 A/m (~ 50 mT, corresponding to the coercivity of ~ 25 mT) and an experimental observation time of 60 s in this work. Also, we assumed H_K to be controlled by shape anisotropy, which is commonly observed in both natural rocks [e.g., Thompson and Oldfield, 1986] and synthetic iron oxides [e.g., Yu *et al.*, 2002].

2.4. X-ray Absorption Near Edge Structure (XANES)

[13] XANES was used to search for tetrahedrally coordinated iron. Fe *K*-edge XANES spectra were recorded at room temperature at the ESRF on the undulator beamline ID26 operating at 6 GeV in 16-bunch mode. A fixed-exit Si (311) double-crystal monochromator was used. The energy was calibrated by defining the first derivative peak of a metallic Fe reference foil to be 7112.0 eV. Two Si mirrors were used for harmonics rejection in the incident X-ray beam. XANES data were recorded in the quick-scan mode by simultaneously

scanning the monochromator angle and the undulator gap with a typical energy step of 0.1 eV in the pre-edge region. The spectra were acquired in the fluorescence mode, using a Si photo-diode. The incident flux was monitored by detecting the X-ray scattering from a thin Kapton foil in the incident beam path. The sample was positioned at 45° with respect to the beam. We measured 2-line ferrihydrite, the intermediate product aged for 90 days and hematite aged for 120 days.

[14] Experimental XANES spectra were reduced by background subtraction with a linear function and then normalized for atomic absorption on the average absorption coefficient for the spectral region from 7150 to 7250 eV. The threshold energy was taken to be the first maximum in the first derivative spectra. Pre-edge peak analysis was carried out according to Wilke *et al.* [2001]. The pre-edge peak was fitted by using a combination of pseudo-Voigt functions. The integrated intensities were compared with those of reported model compounds [Farges, 2001; Wilke *et al.*, 2001] in order to extract information on the coordination number in the studied samples.

3. Results

3.1. Magnetic Results

[15] Aging phosphated ferrihydrite at 150°C caused the susceptibility (Figure 1a) and M_s (Figure 1b) to gradually increase with time, albeit at disparate rates. The re-measured susceptibility results were consistent with those of Barrón and Torrent [2002]. For example, the susceptibility increased from $\sim 1.5 \times 10^{-6} \text{ m}^3 \text{ kg}^{-1}$ for the initial 2-line ferrihydrite to $>250 \times 10^{-6} \text{ m}^3 \text{ kg}^{-1}$ for the 90-day product, and then dropped sharply by several orders of magnitude at day 120, which suggests a fast transformation from strongly magnetic hydromaghemite into weakly magnetic hematite [Barrón and Torrent, 2002].

[16] The hysteresis loop for the initial 2-line ferrihydrite exhibited a linear pattern typical of a paramagnetic substance (Figure 2a). However, the intermediate products obtained for up to 90 days, exhibited a gradually forming ferrimagnetic phase (Figures 2b–2e). Finally, the 120-day product exhibited a completely different hysteretic behavior (Figure 2f). The very high coercivity (~ 250 mT) observed clearly shows that the dominant magnetic carrier is an antiferromagnetic mineral (hematite and/or goethite).

[17] Figure 3 shows the variation of the hysteretic behavior (after correcting for the paramagnetic contributions) of the 7-, 30- and 90-day products. Aging caused the initial susceptibility to gradually increase and loops to become wider; this suggests that the products contained a small fraction of single domain (SD) particles, which possess significant coercivity. This in turn suggests that the grain size of the ferrimagnetic components systematically increases with aging, but the dominant grain size still falls in the SP grain size region.

[18] In order to accurately trace grain size changes, the low-T DC χ -T curves for these samples were compiled in the graph of Figure 4. The initial 2-line ferrihydrite (Figure 4a) and the intermediate products obtained for up to 90 days (Figures 4b–4e) gave similar warming curves in that the DC susceptibility gradually increased to a maximum at $\langle T_B \rangle$ and then decreased with further increase in the temperature up to 300 K. The 120-day product exhibited a rather

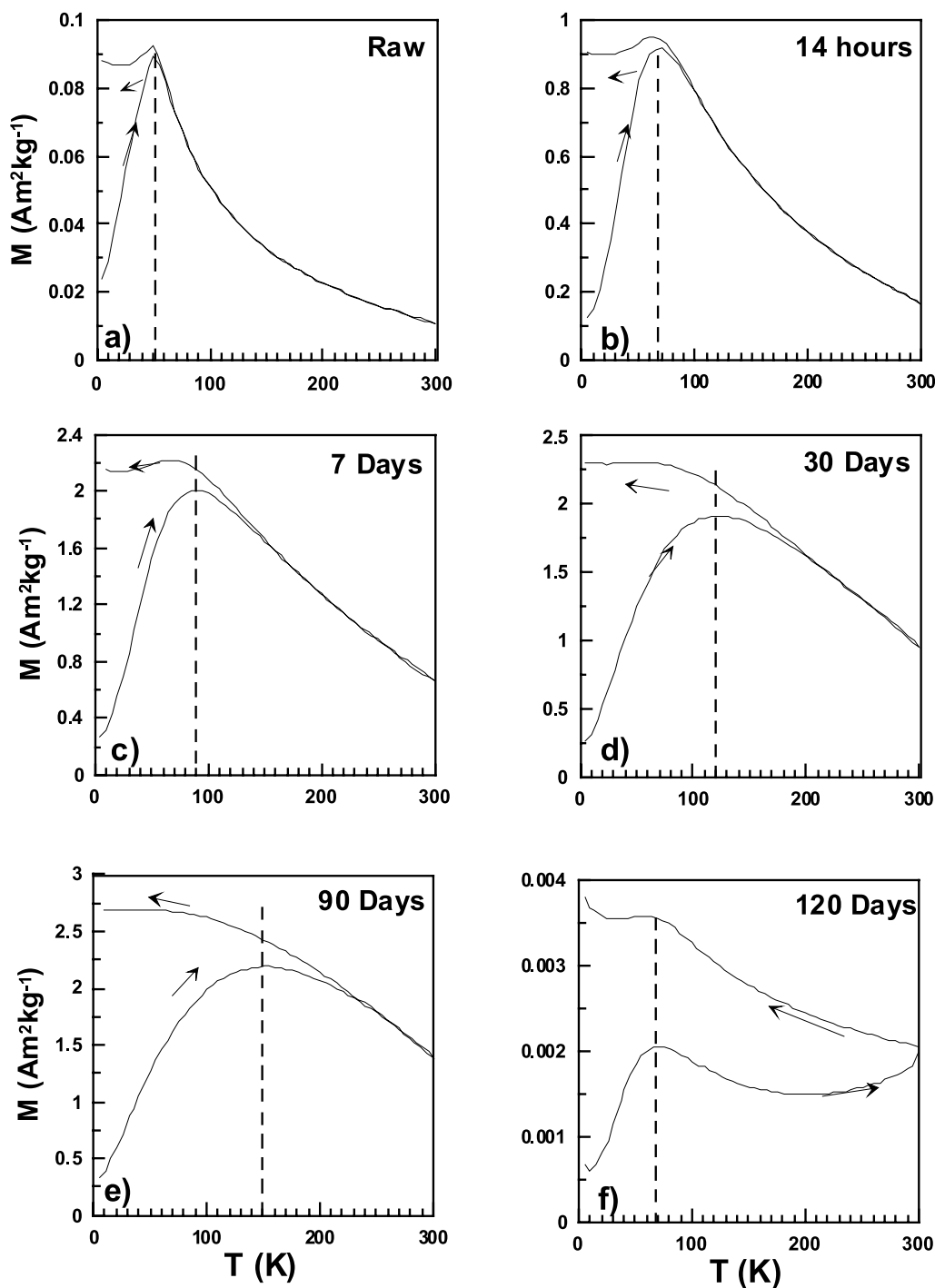


Figure 4. Low-T DC magnetic susceptibility curves for different intermediate products. The dashed lines mark the average unblocking temperature $\langle T_B \rangle$.

different behavior (Figure 4f). Thus the first susceptibility peak at ~ 80 K resembled that for the 12-h product. However, the DC susceptibility increased above ~ 200 K, so the sample must contain a fraction of SD particles that were still blocked at 300 K. The cooling curves were always higher than the warming curves by effect of additional thermal remanent magnetization being acquired during the warming/cooling cycle.

[19] The low-T DC χ - T warming curves for the 12-h, 7-, 30- and 90-day products are shown in Figure 5. $\langle T_B \rangle$ shifted to

higher temperatures with time. The susceptibility maximum at $\langle T_B \rangle$ for the 12-h product was much lower than that for the 7-, 30- and 90-day products, which exhibited similar values. A linear correlation ($R^2 = 0.97$) between the room temperature susceptibility and the corresponding $\langle T_B \rangle$ for the 12-h, 7-, 30- and 90-day products was observed (Figure 6a). On the basis of $\langle T_B \rangle$, the grain size of the particles in the 7-, 30- and 90-day products was estimated to be about 15, 17 and 19 nm, respectively (Figure 6b). This is consistent with the TEM

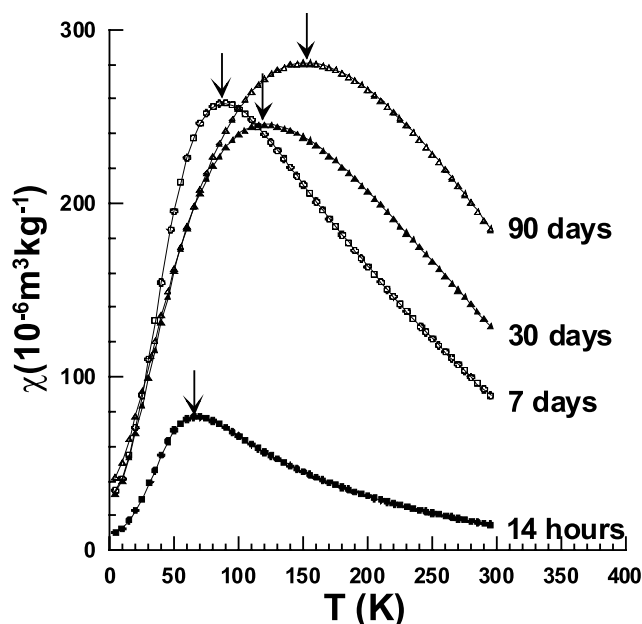


Figure 5. Comparisons of the low-T DC χ - T curves for the intermediate products. Note that the Y axis is scaled on mass-specific χ units. Arrows mark the average unblocking temperature $\langle T_B \rangle$.

observations of Barrón and Torrent [2002] that the grain size of the 90-day products ranged from 10 to 30 nm, but variations in $\langle T_B \rangle$ is more sensitive than the TEM observations.

[20] The increase in grain size with time was also evident from the decrease in SSA: from $288 \text{ m}^2 \text{ g}^{-1}$ for the initial ferrihydrite to 285, 217, 179, 100, and $22 \text{ m}^2 \text{ g}^{-1}$ at 12 h and 7, 30, 90, and 120 days, respectively. On the basis of the densities of maghemite (4.7 kg dm^{-3}) and hematite (5.3 kg dm^{-3}), and on the assumption of equally sized, smooth spherical particles, the 90-day product (mostly hydromaghemite) consisted of particles of $\sim 13 \text{ nm}$, and the 120-day product (hematite) of particles of $\sim 52 \text{ nm}$. However, M_s for the 90-day product was $\sim 5.8 \text{ Am}^2 \text{ kg}^{-1}$, which is only about 7.8% of the theoretical value ($\sim 74 \text{ Am}^2 \text{ kg}^{-1}$, e.g., Özdemir [1990]) for maghemite. This indicates that the

mass effect of ferrihydrite should not be neglected. If we use the density of ferrihydrite ($\sim 4.0 \text{ kg dm}^{-3}$), the estimated particle size for the 90-day product is 15 nm, which is smaller than the estimate based on $\langle T_B \rangle$. However, particles are not spherical and do not have smooth surfaces; therefore, particle size is likely to be significantly greater. Despite these uncertainties about SSA-derived particle size values, one should bear in mind that the changes in SSA clearly indicate that the grain size of magnetic phases increases steadily with aging time.

[21] The stepwise temperature-dependence of the χ curves for the 90-day product is shown in Figure 7. χ was almost reversible at $T_{tr} < 250^\circ\text{C}$ (Figures 7a and 7b), with an ordering temperature of $\sim 130^\circ\text{C}$. By contrast, in the 300 – 350°C run (Figures 7c and 7d), χ decreased significantly and then became relatively reversible at T_{tr} values from 350°C to 500°C (Figures 7e and 7f). In the 600°C (Figure 7g) and 700°C runs (Figure 7h), both the warming curve and the cooling curve exhibited a χ maximum, which corresponds to the unblocking temperature. For the cooling curves, the unblocking temperature gradually increases from $\sim 50^\circ\text{C}$ (Figure 7f) to $\sim 140^\circ\text{C}$ (Figure 7g), and then to $\sim 200^\circ\text{C}$ (Figure 7f) when T_{tr} increases from 500 to 700°C . Moreover, the maximum χ values at the unblocking temperatures gradually decrease. This indicates that the finer-grained fraction was gradually consumed after stepwise heating.

[22] The stepwise M - T curves for the 90-day product (Figure 8) exposed three Curie temperatures: $\sim 70^\circ\text{C}$, 120°C (Figure 8b) and 400°C (Figure 8h). This indicates that the 90-day product contains several magnetic components. Among these three phases, the dominant phase is the last one, which contributes to $> 50\%$ of M_s (Figure 8f). With increasing the T_{tr} , the M_s at the room temperature gradually decreases (Figures 8f–8i), which indicates that this phase is thermally unstable. This is consistent with the results from the χ - T results (Figure 7).

[23] To better address the thermal instability of the magnetic phases in the intermediate product, the ratios of the post-heating M (M_{ph}) and χ (χ_{ph}) to the pre-heating M (M_i) and χ (χ_i) for the 30- and 90-day products are shown in Figure 9. These two samples have disparate M_i and χ_i

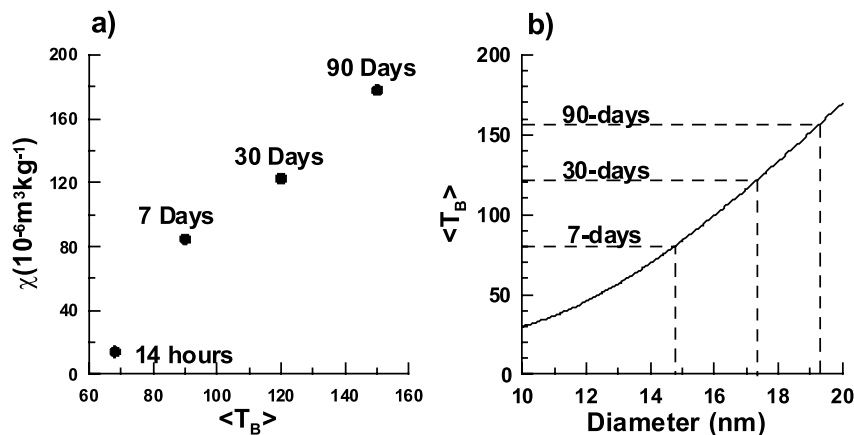


Figure 6. (a) Correlation between the room temperature susceptibility and average unblocking $\langle T_B \rangle$ obtained from Figure 5. (b) Correlation between $\langle T_B \rangle$ and the diameter of maghemite particles with the room-T coercivity of 25 mT. The dashed lines in (b) indicate different 7-, 30- and 90-day products.

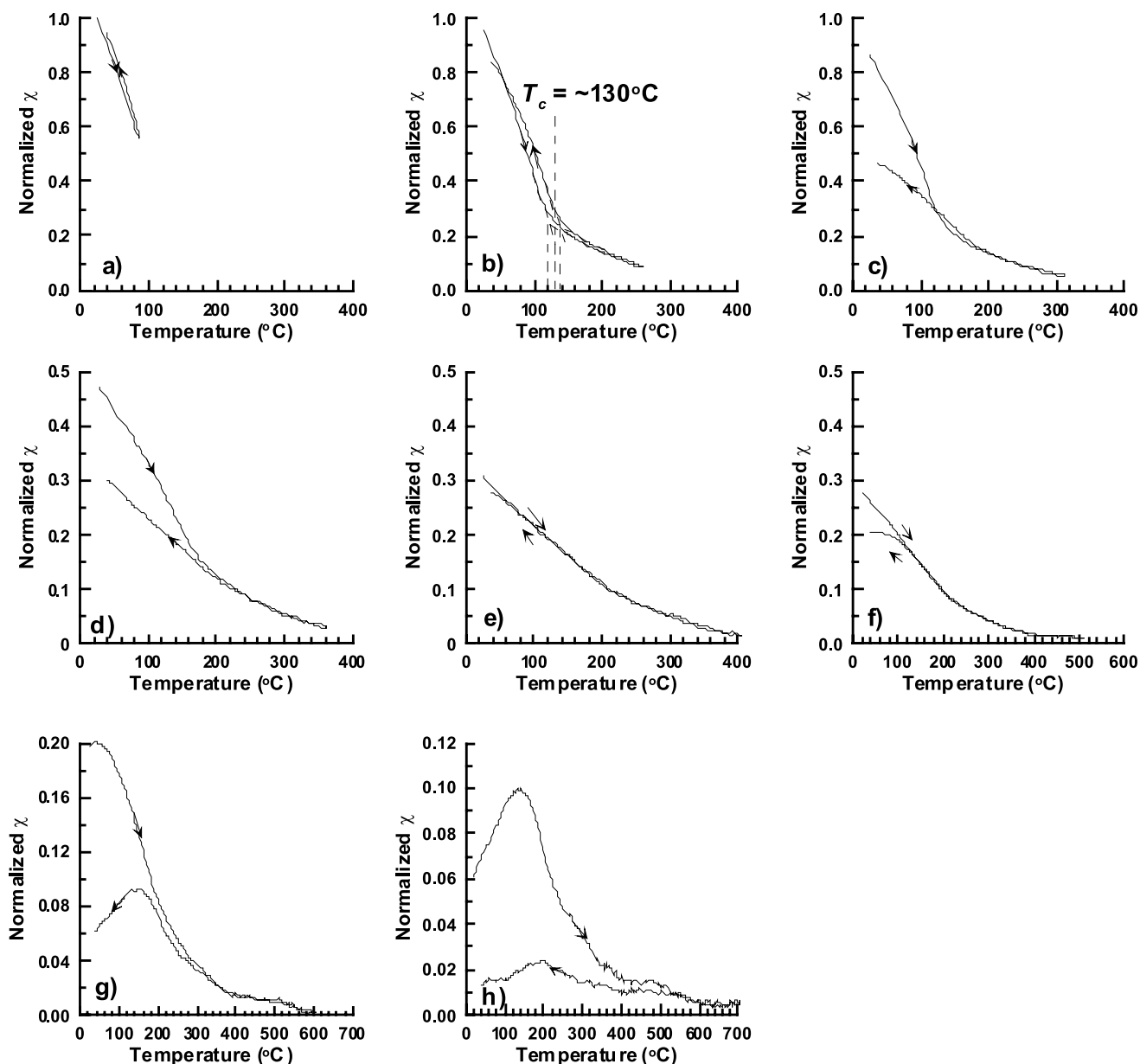


Figure 7. (a–h) Temperature-dependence of χ for the 90-day product. Arrows indicate the heating/cooling cycles.

values, but similar $M_{\text{ph}}/M_{\text{I}}$ and $\chi_{\text{ph}}/\chi_{\text{I}}$ patterns with respect to T_{tr} . This indicates that the magnetic enhancement in the 30- and 90-day products is mainly the result of changes in concentration of the newly formed magnetic minerals. The large decrease in both M and χ at T_{tr} values from 250 to 350°C indicates that a strongly magnetic phase has been transformed into a weakly magnetic phase. This mineral transformation corresponds to the gradual removal of the phase with a Curie temperature (T_{c}) of 130°C rather than the thermally relatively stable phase with $T_{\text{c}} \sim 400^\circ\text{C}$, which was gradually transformed into a weakly magnetic phase at elevated temperatures ($>350^\circ\text{C}$).

3.2. XANES Spectra

[24] The normalized Fe K -edge XANES spectra for 2-line ferrihydrite, the intermediate product aged at 90 days, and

hematite aged at 120 days are shown in Figure 10. As can be seen, there are marked differences between hematite and the other samples in the energy region below 7120 eV (the pre-edge region). The peaks in the pre-edge region (pre-edge peaks) constitute a reliable fingerprint for the oxidation state and site symmetry of the iron atoms [e.g., Wilke *et al.*, 2001]. These peaks represent a $1s$ - $3d$ like transition, which is dipole-forbidden but can be partially allowed by mixing of the d -states of the transition metal with the p -states of the surrounding oxygen atoms. Hence spectral intensity arises from dipole and quadrupole transition matrix elements. Electron-electron interactions can give a rich multiplet structure and cause multielectron excitations. A theoretical analysis requires further considering crystal field effects and orbital hybridization. The energy position of the pre-edge feature depends mainly on the mean Fe oxidation state,

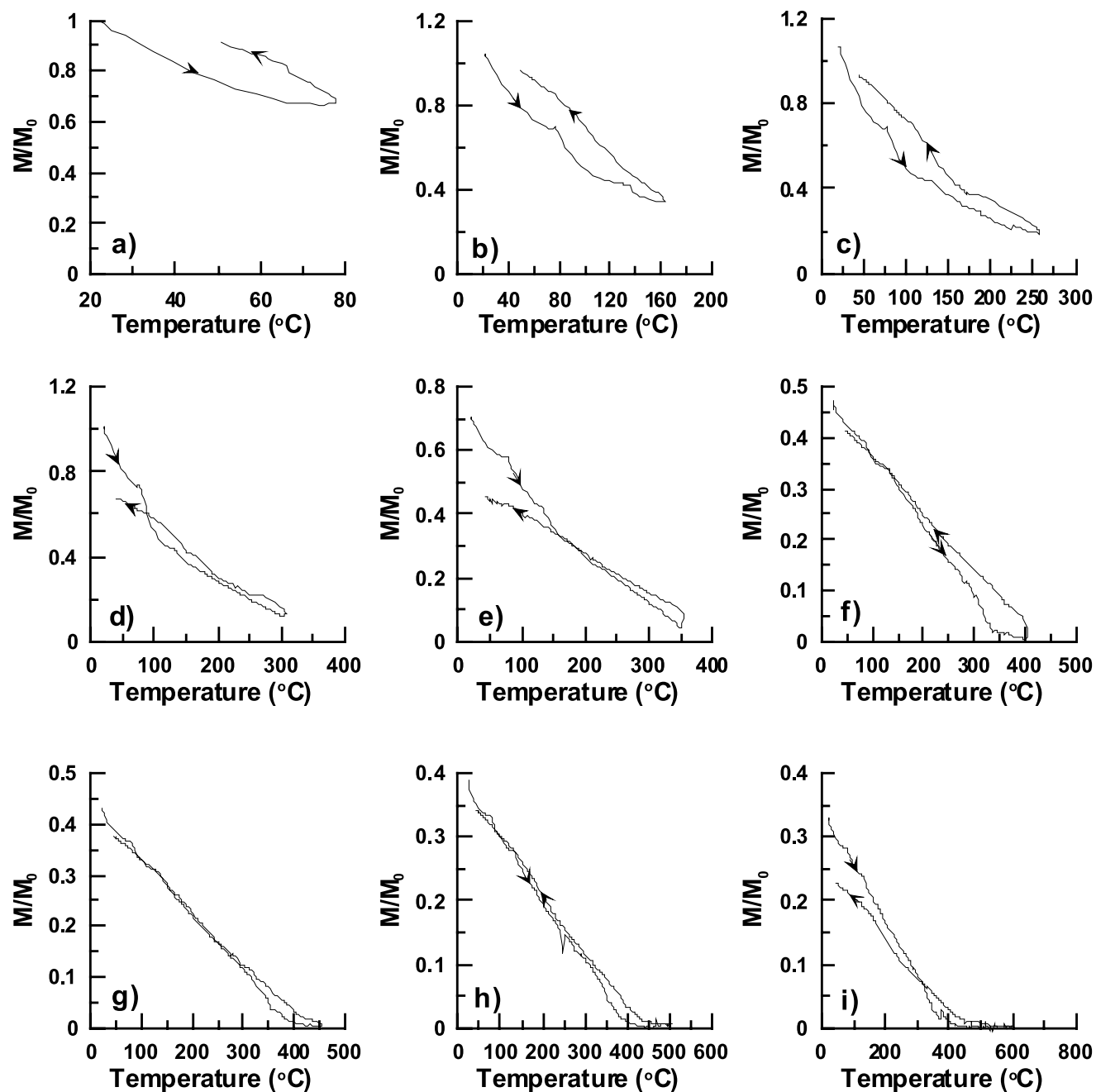


Figure 8. Temperature-dependence of magnetization (M) for the 90-day product. Arrows indicate the heating/cooling cycles. The applied field was 300 mT.

which gradually increases from Fe^{2+} to Fe^{3+} . The intensity of the pre-edge feature depends on the geometry around Fe [Calas and Petiau, 1983; Wilke et al., 2001]; it is near zero with a regular octahedral symmetry around the absorber and maximal with tetrahedral coordination.

[25] Table 1 shows the normalized height and position of the pseudo-Voigts for the studied samples. Obviously, our samples only contained ferric iron (energy position of the centroid at ~ 7114.4 eV). The separation of ~ 1.2 – 1.3 eV between the two pre-edge peaks in hematite is related to the splitting into e_g - and t_{2g} -like components and typical of high-spin ferric complexes of O_h geometry [Westre et al., 1997]. The additional pre-edge component observed in the

oxides results from processes other than a $1s \rightarrow 3d$ transition and probably involving Fe second neighbors [Wilke et al., 2001]. Close inspection of Figure 10 reveals that 2-line ferrihydrite has a strongly asymmetric pre-edge peak with a shoulder on the low-energy side. This peak becomes less asymmetric in the intermediate products and has a higher integrated intensity (Table 1). Ferric iron in tetrahedral coordination gives a narrow, symmetric, strong pre-edge peak [Manceau and Gates, 1997]. Consequently, the pre-edge features for ferrihydrite, both shape and integrated intensity suggest the presence of octahedrally coordinated ferric iron; by contrast, the intermediate product aged for 90 days may contain some tetrahedrally coordinated iron.

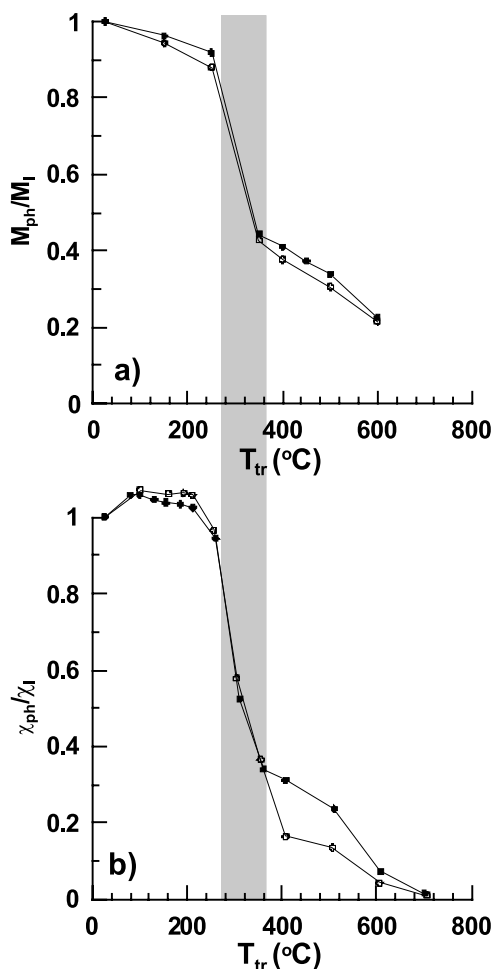


Figure 9. Comparison of the ratio of post-heating χ (χ_{ph}) and M (M_{ph}) to the initial χ (χ_i) and M (M_i) as a function of the treatment temperature (T_{tr}) for the 30-day (open circles) and 90-day (solid circles) products.

The presence of tetrahedrally coordinated iron and the absence of ferrous iron are indicative of the presence of maghemite in the intermediate product.

4. Discussion

4.1. Magnetic Phases in the Intermediate Products

[26] The stepwise χ - T and M - T warming curves for the 90-day products reveal two major magnetic phases with ordering temperatures of about 120°C and 400°C (Figures 7 and 8), respectively. The first ordering temperature might correspond to goethite or ferrihydrite. Since goethite displays two separate XANES pre-edge peaks [O'Day *et al.*, 2004; Wilke *et al.*, 2001], the single pre-edge peak (Figure 10) excludes the presence of goethite. The X-ray diffraction and Mössbauer spectra also confirmed that the dominant antiferromagnetic phase in the intermediate products was hematite rather than goethite [Barrón *et al.*, 2003].

[27] There is some controversy over the Néel temperature (T_N) of ferrihydrite. At room temperature, pure ferrihydrite has been reported to be paramagnetic because its Néel temperature (T_N) are well below 300 K [Zergenyi *et al.*, 2000]. However, by linearly extrapolating the induced

magnetization curve, Berquó *et al.* [2007] estimated T_N for Si-ferrihydrite to be about 422 K, which is consistent with our results. This is a result of P being probably incorporated into tetrahedral positions during aging to form P-ferrihydrite, which may thus resemble the Si-ferrihydrite studied by Berquó *et al.* [2007]. Therefore the 120°C ordering temperature indicates that ferrihydrite still exists in the 90-day product.

[28] Based on Mössbauer spectra and X-ray diffraction patterns, Barrón and Torrent [2002] and Barrón *et al.* [2003] concluded that maghemite is the dominant ferrimagnetic phase responsible for magnetic enhancement in the intermediate products. The XANES spectra (Figure 10) indicate that some tetrahedrally coordinated ferric iron is present in the intermediate product, hence confirming the presence of maghemite. Moreover, Figures 7 and 8 show that the ferrimagnetic component with a $T_c \sim 400^\circ\text{C}$ is thermally unstable at $T_{tr} > 350^\circ\text{C}$. This is also a typical property of maghemite, which is generally transformed into hematite at elevated temperatures [de Boer and Dekkers, 1996]. A maghemite phase of low T_c (470–475°C) has been reported by Takei and Chiba [1966] and de Boer and Dekkers [2001]. This maghemite variety exhibits vacancies at tetrahedral sites, which distinguishes it from the common maghemite forms [de Boer and Dekkers, 2001].

[29] In summary, the 60- and 90-day intermediate products with enhanced magnetic properties consist of ferrihydrite, maghemite and hematite. Their magnetic enhancement is mostly due to the neoformation of maghemite of low T_c .

4.2. Paleoenvironmental Implications

[30] Ferrihydrite is a common iron oxyhydroxide mineral in a wide range of natural environments [Schwertmann,

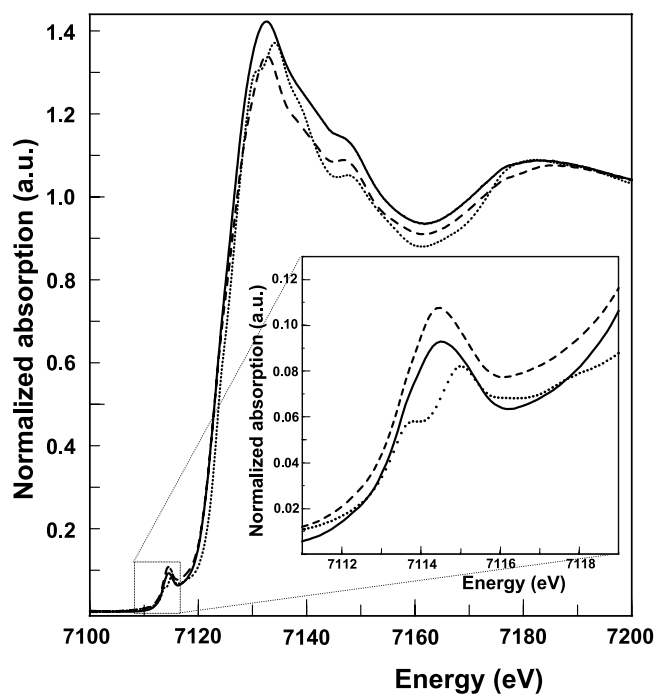


Figure 10. K -edge XANES for 2-line ferrihydrite (solid line), the intermediate phase aged for 90 days (dashed line) and hematite (dotted line). The inset is a magnified view of the pre-edge.

Table 1. Pre-edge Characteristics of the Studied Samples

Sample	Normalized Height, a.u.	Component Position, eV	Width, eV	Area, a.u.	Total Area, a.u.	Centroid Position, eV
Raw 2-line ferrihydrite	0.03	7113.88	1.11	0.07	0.1678	7114.50
	0.04	7114.68	1.11	0.09		
	0.01	7115.58 ^a	1.11	0.02		
120 days product (hematite)	0.04	7113.72	1.57	0.05	0.1473	7115.39
	0.07	7115.04	1.57	0.10		
	0.03	7116.50 ^a	1.57	0.04		
	0.02	7117.93 ^a	1.57	0.03		
	0.09	7114.37	1.32	0.19		
Intermediate phase 90 days	0.02	7116.11	1.32	0.03	0.2090	7114.63

^aThese pre-edge components result from processes other than 1s→3d transitions probably involving iron second neighbors [Wilke *et al.*, 2001].

1988] such as the water column of lakes [Tipping and Onstad, 1981], sediments [Chukhrov, 1973], and soils [Campbell and Schwertmann, 1984]. Dearing *et al.* [1996] systematically investigated magnetic properties for topsoils across England and found magnetic enhancement in topsoils to be directly related to the Fe supply from weathering within the soil. They further proposed that ferrihydrite is the most important precursor for other secondary magnetic minerals (e.g., magnetite and maghemite) formed through pedogenesis.

[31] As can be seen from Figure 6, room temperature χ is proportional to $\langle T_B \rangle$, which indicates that grain size of maghemite increases with aging. The transformation of maghemite into hematite occurs when the maghemite particles grow into the SD region; therefore, the grain size of maghemite is critical parameter for this transformation. If this is true, we can predict that hematite formed from ferrihydrite must fall in the SD region or that only the larger ferrihydrite particles have the potential for forming hematite. This is consistent with results for natural samples. For example, the mean coherence length in the normal direction to the (110) crystal plane of hematite in soils of Mediterranean and tropical regions generally falls in the 25–50 nm size range, i.e., the SD grain size region [Torrent, 1994; Cornell and Schwertmann, 2003].

[32] Interpreting our results is easier if one considers some observations on hematite and the analogous Al oxide. So, McHale *et al.* [1997] reported the presence of a γ -Al₂O₃ phase on the surface of nano-sized corundum (α -Al₂O₃) and, according to Chernyshova *et al.* [2007], nano-sized hematite often possesses maghemite-like (γ -Fe₂O₃) defects in the near surface regions. This is a result of maghemite having a lower surface energy than hematite [Chernyshova *et al.*, 2007]. Moreover, the stability of maghemite-like surface defects decreases with increasing particle size and, beyond a given threshold (e.g., several tens of nm), the maghemite-like phase is completely transformed into hematite [Chernyshova *et al.*, 2007]. This model can seemingly be applied to our ferrihydrite → hydromaghemite → hematite system, where, based on XRD analysis [Barrón and Torrent, 2002; Barrón *et al.*, 2003], the hydromaghemite phase contains structural OH and exhibits structural defects.

[33] The proposed pathway is consistent with the known relationships between some magnetic properties and the Fe oxide mineralogy of soils and paleosols in various regions. It should be noted that the above-discussed pathway is temperature dependent [Barrón and Torrent, 2002]. Our

experiments were carried out at above-ambient temperatures in order to ensure reasonably high transformations rates. The time required to reach the susceptibility maximum increased from ~0.9 day at 200°C to ~5 days at 175°C, and then to ~90 days at 150°C. Below 100°C, no significant formation of hematite was observed over the studied period. However, by extrapolating the Arrhenius plot fitted to the data from 150 to 200°C, Barrón and Torrent [2002] estimated the time for the transformation from maghemite into hematite to be about 1 Ma at room temperature, thus significantly extending the laboratory timescales to geological time. The accuracy of this extrapolation is indeed limited because the transformation of ferrihydrite is likely to be affected by many soil environmental factors (pH, inorganic and organic ligands, water activity); in any case, it suggests that maghemite can be a stable magnetic phase during pedogenesis. Our model is consistent with the observation that soils developed under warm climates are more magnetically enhanced and contain more hematite than those under cool climates, where ferrihydrite has evolved mostly to goethite [Torrent *et al.*, 2006]. For instance, one recent study on the Chinese loess/paleosol Luochuan sequence [Torrent *et al.*, 2007] showed paleosols to be richer in pedogenic hematite than in pedogenic goethite, and magnetic enhancement and hematite content to be highly correlated. In summary, the ferrihydrite → maghemite → hematite pathway plays a key role in the mineralogical evolution of Fe oxides during pedogenesis, at least in some environments.

[34] If the proposed ferrihydrite → hydromaghemite → hematite transformation model applies to soil, then the particle size distribution of maghemite is likely to depend on the rates of (1) weathering of Fe-bearing minerals to produce ferrihydrite; (2) transformation of ferrihydrite into hydromaghemite; (3) growth of hydromaghemite particles; and (4) transformation of hydromaghemite into hematite. Also, steps (2) and (3) are expected to be influenced by the concentration of phosphate and other ligands in the soil solution. In soils containing weatherable Fe-bearing minerals, one can expect continuous formation of ferrihydrite provided the temperature and moisture conditions are favorable; therefore, all intermediate stages in the formation (and growth) of maghemite are likely to be represented, thereby resulting in a wide grain size distribution of maghemite. In this environment, such a distribution of pedogenically produced maghemite particles might be insensitive to the degree of pedogenesis [Liu *et al.*, 2004b, 2005b; Geiss and Zanner, 2006]. By contrast, in highly weathered soils, where the

supply of ferrihydrite is negligible, one can expect the initial products of its transformation (viz. fined grained hydromaghemite) to be substantially less abundant than the final products (viz. coarse grained hydromaghemite and hematite). This hypothesis should be tested in future studies.

5. Conclusions

[35] The main conclusion of our study is that hydromaghemite can be directly formed from ferrihydrite and eventually becomes hematite at the stage where the volume of hydromaghemite particles increases from values in the superparamagnetic region to levels in the single-domain region. Goethite is not directly associated with this process. The transformation pathway (ferrihydrite \rightarrow SP maghemite \rightarrow SD maghemite \rightarrow SD hematite) is consistent with some features of pedogenesis, and may thus be largely responsible for magnetic enhancement in various types of soil.

[36] **Acknowledgments.** Q.S. Liu was supported by the European Commission through a Marie-Curie Fellowship (IIF), proposal number 7555. The contribution of J. Torrent and V. Barrón was supported by the Spain's Ministerio de Ciencia y Tecnología, Project AGL2003-01510. C. Deng was supported by the NSFC grants 40674032, 40221402 and 40325011, and CAS grant KZCX-3-SW-150. We acknowledge the European Synchrotron Radiation Facility for provision of synchrotron radiation facilities and we would like to thank the staff of beamline ID26.

References

- Banin, A., T. Ben-Shlomo, L. Margulies, D. F. Blake, R. L. Mancinelli, and A. U. Gehring (1993), The nanophase iron mineral(s) in Mars soil, *J. Geophys. Res.*, *98*, 20,831–20,835.
- Barrón, V., and J. Torrent (2002), Evidence for a simple pathway to maghemite in Earth and Mars soils, *Geochim. Cosmochim. Acta.*, *66*, 2801–2806.
- Barrón, V., J. Torrent, and E. de Grave (2003), Hydromaghemite, an intermediate in the hydrothermal transformation of 2-line ferrihydrite into hematite, *Am. Mineral.*, *88*, 1679–1688.
- Berquó, T. S., S. K. Banerjee, R. G. Ford, R. L. Penn, and T. Pichler (2007), High crystallinity Si-ferrihydrite: An insight into its Néel temperature and size dependence of magnetic properties, *J. Geophys. Res.*, *112*, B02102, doi:10.1029/2006JB004583.
- Calas, G., and J. Petiau (1983), Coordination of iron in oxide glasses through High-Resolution K-Edge Spectra - Information from the Pre-Edge, *Solid State Commun.*, *48*, 625–629.
- Campbell, A. S., and U. Schwertmann (1984), Iron oxide mineralogy of plagic horizons, *Soil Sci.*, *35*, 5–69.
- Chernyshova, I. V., M. F. Hochella, and A. S. Madden (2007), Size-dependent structural transformations of hematite nanoparticles. 1. Phase transition, *Phys. Chem. Chem. Phys.*, *9*, 1736–1750.
- Chukhrov, F. V. (1973), On mineralogical and geochemical criteria in the genesis of red bed, *Chem. Geol.*, *12*, 67–75.
- Cornell, R. M., and U. Schwertmann (2003), *The Iron Oxides*, 2nd. ed., Wiley-WCH, Weinheim, Germany.
- Dearing, J. A., K. Hay, S. Baban, A. S. Huddleston, E. M. H. Wellington, and P. J. Loveland (1996), Magnetic susceptibility of topsoils: A test of conflicting theories using a national database, *Geophys. J. Int.*, *127*, 728–734.
- de Boer, C. B., and M. J. Dekkers (1996), Grain-size dependence of the rock magnetic properties for a natural maghemite, *Geophys. Res. Lett.*, *23*, 2815–2818.
- de Boer, C. B., and M. J. Dekkers (2001), Unusual thermomagnetic behavior of haematites: Neof ormation of a highly magnetic spinel phase on heating in air, *Geophys. J. Int.*, *144*, 481–494.
- Dunlop, D. J., and Ö. Özdemir (1997), *Rock Magnetism: Fundamentals and Frontiers*, Cambridge Univ. Press, New York.
- Eggleton, R. A., and R. W. Fitzpatrick (1988), New data and a revised structural model for ferrihydrite, *Clays Clay Mineral.*, *36*, 111–124.
- El-Hilo, M., K. O'Grady, and R. W. Chantrell (1992), Susceptibility phenomena in a fine particle system. I. Concentration dependence of the peak, *J. Magn. Magn. Mater.*, *114*, 295–306.
- Farges, F. (2001), Crystal chemistry of iron in natural grandidierites: An X-ray absorption fine-structure spectroscopy study, *Phys. Chem. Miner.*, *28*, 619–629.
- Geiss, C. E., and C. W. Zanner (2006), How abundant is pedogenic magnetite? Abundance and grain size estimates for loessic soils based on rock magnetic analyses, *J. Geophys. Res.*, *111*, B12S21, doi:10.1029/2006JB004564.
- Gittleman, J. I., B. Abelas, and S. Bozowski (1974), Superparamagnetism and relaxation effects in granular Ni-SiO₂ and Ni-Al₂O₃ films, *Phys. Rev.*, *B9*, 3891–3897.
- Jackson, M., and H.-U. Worm (2001), Anomalous unblocking temperatures, viscosity and frequency-dependency susceptibility in the chemically remagnetized Trenton limestone, *Phys. Earth Planet. Inter.*, *126*, 27–42.
- Janney, D. E., J. M. Cowley, and P. R. Buseck (2000), Structure of synthetic 2-line ferrihydrite by electron nanodiffraction, *Am. Mineral.*, *85*, 1180–1187.
- Khater, A., J. Ferre, and P. Meyar (1987), Spin-cluster theory in magnetic materials and applications to spin glasses, *J. Phys.*, *20*, 1857–1865.
- Liu, Q. S., S. K. Banerjee, M. J. Jackson, C. L. Deng, Y. X. Pan, and R. X. Zhu (2004a), New insights into low-temperature oxidation of magnetites and thermal alteration of magnetic mineralogy of the Chinese loess in air, *Geophys. J. Int.*, *158*, 506–514.
- Liu, Q. S., M. J. Jackson, Y. J. Yu, F. H. Chen, C. L. Deng, and R. X. Zhu (2004b), Grain size distribution of pedogenic magnetic particles in Chinese loess/paleosols, *Geophys. Res. Lett.*, *31*, L22603, doi:10.1029/2004GL021090.
- Liu, Q. S., M. J. Jackson, S. K. Banerjee, B. A. Maher, C. L. Deng, Y. X. Pan, and R. X. Zhu (2005a), Mechanism of the magnetic susceptibility enhancements of the Chinese loess, *J. Geophys. Res.*, *110*, B12107, doi:10.1029/2004JB003249.
- Liu, Q. S., J. Torrent, B. A. Maher, Y. Yu, C. L. Deng, R. X. Zhu, and X. X. Zhu (2005b), Quantifying grain size distribution of pedogenic magnetic particles in Chinese loess and its significance for pedogenesis, *J. Geophys. Res.*, *110*, B11102, doi:10.1029/2005JB003726.
- Liu, Q. S., C. L. Deng, J. Torrent, and R. X. Zhu (2007), Review of recent developments in mineral magnetism of the Chinese loess, *Quat. Sci. Rev.*, *26*, 368–385.
- Maher, B. A. (1986), Characterization of soils by mineral magnetic measurements, *Phys. Earth Planet. Inter.*, *42*, 76–91.
- Maher, B. A. (1998), Magnetic properties of modern soils and Quaternary loessic paleosols: Paleomagnetic implications, *Palaeogeogr. Palaeoclimatol. Palaeoecol.*, *137*, 25–54.
- Manceau, A., and W. P. Gates (1997), Surface structural model for ferrihydrite, *Clays Clay Miner.*, *45*, 448–460.
- Mazzetti, L., and P. J. Thistlethwaite (2002), Raman spectra and thermal transformations of ferrihydrite and schwertmannite, *J. Raman Spectrosc.*, *33*, 104–111.
- McHale, J. M., A. Auroux, A. J. Perrotta, and A. Navrotsky (1997), Surface energies and thermodynamic phase stability in nanocrystalline aluminas, *Science*, *277*, 788–791.
- Michel, F. M., L. Ehm, S. M. Antao, P. L. Lee, P. J. Chupas, G. Liu, D. R. Strongin, M. A. A. Schoonen, B. L. Phillips, and J. B. Parise (2007a), The structure of ferrihydrite, a nanocrystalline material, *Nature*, *316*, 1726–1729.
- Michel, F. M., et al. (2007b), Similarities in 2- and 6-line ferrihydrite based on pair distribution function analysis of X-ray total scattering, *Chem. Mater.*, *19*, 1489–1496.
- Morris, R. V., D. C. Golden, T. D. Shelfer, and J. H. V. Lauer (1998), Lepidocrocite to maghemite to hematite: A pathway to magnetic and hematitic Martian soil, *Meteorit. Planet. Sci.*, *33*, 743–751.
- Mullins, C. E. (1977), Magnetic susceptibility of the soil and its significance in soil science: A review, *J. Soil Sci.*, *28*, 223–246.
- Murad, E., and U. Schwertmann (1993), Temporal stability of a fine-grained magnetite, *Clays Clay Mineral.*, *41*, 111–113.
- O'Day, P. A., N. Rivera, R. Root, and S. A. Carroll (2004), X-ray absorption spectroscopic study of Fe reference compounds for the analysis of natural sediments, *Am. Mineral.*, *89*, 572–585.
- Özdemir, Ö. (1990), High-temperature hysteresis and thermoremanence of single-domain maghemite, *Phys. Earth Planet. Inter.*, *65*, 125–136.
- Schwertmann, U. (1988), Occurrence and formation of iron oxide minerals in various pedoenvironments, in *Iron in Soils and Clay Minerals*, edited by J. W. Stucki, B. A. Goodman, and U. Schwertmann, pp. 267–308, D. Reidel, Norwell, MA.
- Schwertmann, U., and R. M. Taylor (1989), Iron oxides, in *Minerals in Soil Environments*, edited by J. B. Dixon and S. B. Weed, pp. 379–438, Soil Sci. Soc. Am., Madison, WI.
- Singer, M. J., K. L. Verosub, P. Fine, and J. Tenpas (1996), A conceptual model for the enhancement of magnetic susceptibility in soils, *Quat. Int.*, *34–36*, 243–248.
- Takei, H., and S. Chiba (1966), Vacancy ordering in epitaxially-grown single crystals of γ -Fe₂O₃, *J. Phys. Soc. Jpn.*, *45*, 1255–1263.
- Thompson, R., and F. Oldfield (1986), *Environmental Magnetism*, Allen and Unwin, St. Leonards, NSW, Australia.
- Tipping, E., and M. Onstad (1981), Iron oxide from a seasonally anoxic lake, *Geochim. Cosmochim. Acta*, *45*, 1411–1419.

- Torrent, J. (1994), Iron oxides in Mediterranean soils: properties and influence on soil behaviour, in *Transactions, 15th World Congress of Soil Science*, Acapulco, Mexico, pp. 2–14, Volume 8.
- Torrent, J., V. Barrón, and Q. S. Liu (2006), Magnetic enhancement is linked to and precedes hematite formation in aerobic soil, *Geophys. Res. Lett.*, *33*, L02401, doi:10.1029/2005GL024818.
- Torrent, J., Q. S. Liu, J. Bloemendal, and V. Barrón (2007), Magnetic enhancement and iron oxides in the Upper Luochuan loess-paleosol sequence, Chinese Loess Plateau, *Soil Sci. Soc. Am. J.*, *71*, 1570–1578.
- van Velzen, A. J., and M. J. Dekkers (1999a), The incorporation of thermal methods in mineral magnetism of loess-paleosol sequences: A brief overview, *Chinese Sci. Bull.*, *44*, 53–63.
- van Velzen, A. J., and M. J. Dekkers (1999b), Low-temperature oxidation of magnetite in loess-paleosol sequences: A correction of rock magnetic parameters, *Stud. Geophys. Geod.*, *43*, 357–375.
- Verosub, K. L., P. Fine, M. J. Singer, and J. TenPas (1993), Pedogenesis and paleoclimate: Interpretation of the magnetic susceptibility record of Chinese loess-paleosol sequences, *Geology*, *21*, 1011–1014.
- Westre, T. E., P. Kennepohl, J. G. DeWitt, B. Hedman, K. O. Hodgson, and E. I. Solomon (1997), A multiplet analysis of Fe K-edge 1s→3d pre-edge features of iron complexes, *J. Am. Chem. Soc.*, *119*, 6297–6314.
- Wilke, M., F. Farges, P. E. Petit, G. E. Brown, and F. Martin (2001), Oxidation state and coordination of Fe in minerals: An Fe K-XANES spectroscopic study, *Am. Mineral.*, *86*, 714–730.
- Yu, Y., D. J. Dunlop, and Ö. Özdemir (2002), Partial anhysteretic remanent magnetization in magnetite: 1. Additivity, *J. Geophys. Res.*, *107*(B10), 2244, doi:10.1029/2001JB001249.
- Zergenyi, R. S., A. M. Hirt, S. Zimmermann, J. P. Dobson, and W. Lowrie (2000), Low-temperature magnetic behavior of ferrihydrite, *J. Geophys. Res.*, *105*, doi:10.1029/1999JB900315.

V. Barrón and J. Torrent, Departamento de Ciencias y Recursos Agrícolas y Forestales, Universidad de Córdoba, Edificio C4, Campus de Rabanales, 14071 Córdoba, Spain.

C. Deng, Paleomagnetism and Geochronology Laboratory (SKL-LE), Institute of Geology and Geophysics, Chinese Academy of Sciences, Beijing 100029, China.

S. G. Eeckhout, European Synchrotron Radiation Facility (ESRF), 6 rue Jules Horowitz, BP 220, 38043, Grenoble, France.

Q. Liu, National Oceanography Centre, University of Southampton, European way, Southampton, SO14 3ZH, UK. (liux0272@yahoo.com)